Article

Performance Improvement During Attitude Motion of a Vehicle Using Aerodynamic Surfaces based Anti-jerk Predictive Controller

Ejaz Ahmad and Iljoong Youn *

[1] Department of Mechanical and Aerospace Engineering, Gyeongsang National University, ReCAPT, Jinju, Gyeongnam 52828, Korea; ejaz.msee@gmail.com

* Correspondence: iyoun@gnu.ac.kr; Tel.: +82-55-772-1627

Abstract: This paper presents designing an attitude motion control strategy for a half-car model using an anti-jerk predictive controller. Anti-jerk predictive controller based on active aerodynamics surfaces is employed to deal with the anticipated future road maneuvers and improve vehicle ride performance by canceling out external jerks acting on the vehicle body. The body jerks are produced during vehicle traversing on a double lane-change maneuver, acceleration, or braking. The control strategy helps the vehicle to achieve a realistic operation of the active aerodynamic surface to improve the vehicle's ride performance, i.e., ride comfort and road holding during cornering, acceleration, or braking. The anti-jerk predictive controller is developed based on the predictive control strategy, which predicts future road inputs and uses them to compensate for the vehicle's attitude motion. The simulation results show that the proposed control strategy effectively reduces the effects of vehicle body jerks transmitted to the passengers, improving ride comfort without degrading vehicle handling. The anti-jerk predictive controller successfully tracks the desired attitude position by canceling the external body jerks.

Keywords: anti-jerk control; predictive control;braking; half-car model; attitude motion tacking; lane-change maneuver;

1. Introduction

The significant advancements achieved to enhance vehicle ride performance over the past few decades have significantly contributed to the automotive industry. The two essential components of a vehicle's ride performance that have received the interest of numerous researchers are ride comfort and road-holding capability [1,2]. Ride comfort is related to the unpleasant vibrations of the vehicle body transmitted to the passengers. Road holding means reducing oscillations in the usual wheel load to improve the tire's traction on the road during different maneuvers [3,4]. Separating these vibrations caused by various factors such as uneven road surfaces, centrifugal forces during cornering, or inertial forces during braking or acceleration on the car's body influences ride performance. [5–7]. Although the ride comfort and vehicle tire traction on the road has substantially increased, automobile engineers are still concerned about driving on various maneuvers. Hence, an appropriate control systems framework is essential that can easily address these two aspects to enhance ride performance. In order to address the trade-off between the two components of ride quality, the research on the applications of aerodynamic surfaces-based control strategies has gained significant impetus to improve vehicle performance.

The applications of active aerodynamic surfaces (AAS) installed on the vehicle sprung mass have attracted automotive engineers to improve ride performance. Active aerodynamic surfaces-based control strategies can significantly increase negative lift force with increased vehicle speed, effectively improving ride performance. Savkoor [8–10] published early primary research on the applications of AAS, using several control

 doi:10.20944/preprints202305.0142.v1

strategies to reduce the heave and pitch angle of a truck cabin. In [11], Doniselli et al. investigated how aerodynamics affected a high-speed car's ride quality on a randomly contoured route. The recent research on sports cars by [12–16] used various control approaches to investigate the applications of AAS to improve ride comfort. Active aerodynamic control (AAC) strategies are also effective in improving the lateral performance of a road vehicle. The AACs are employed to manipulate the aerodynamic surfaces to generate varying negative lift forces to enhance the vehicle's handling capability [17–19]. In our previous work [20], we have analyzed that the aerodynamic surfaces can generate negative lift force to improve the ride quality of a vehicle considering pitch and roll dynamics. Though these researches effectively improve ride performance, their performance depends on AAS's idealistic moments. The major challenge with vehicles equipped with AAS is the realistic motion of aerodynamic surfaces installed on unsprung mass. The negative lift force generated by AAS is useful for increasing the tire grip on the road, but it can be detrimental to ride comfort. Due to high speed, the sharp movement of aerodynamic surfaces will result in high vehicle body jerk and acceleration, severely affecting passenger ride comfort. Therefore, an appropriate solution to reduce the adverse impact of the vehicle body jerk on passengers to ensure better ride comfort and road-holding capability is aimed towards an anti-jerk control strategy.

As discussed by [21], the term "jerk" is considered a better performance parameter for measuring ride comfort than acceleration and is widely used in engineering applications. For example, its consideration as ride comfort parameter in amusement rides [22–24], elevators [25], ships [26] and buses [27]. The jerk is considered an important passenger ride discomfort parameter in vehicles and is extensively discussed in automotive engineering. Anti-jerk controllers are commonly employed in electric vehicles to reduce the longitudinal jerk to enhance ride comfort and drivability [28,29]. Hence, anti-jerk control strategies have inspired many researchers to enhance ride comfort by reducing the longitudinal jerk produced during starting of electric vehicles. A non-linear model predictive-based anti-jerk cruise controller is developed in [30] for electric vehicles to reduce the longitudinal jerk to improve passenger ride comfort. In [31] model predictive anti-jerk controller is developed to overcome the trade-off between ride comfort and vehicle handling. In [32] anti-jerk controller is developed for a hybrid electric vehicle to reduce the jerk produced during the clutch start. To track the intended velocity with the least jerk and improved road safety, [33] employed a linear quadratic-based anti-jerk controller. [34] utilized a low-jerk suspension control technology to improve ride comfort. A backlash-based anti-jerk controller is employed in [35] to reduce the jerk during clutch engagement. However, these anti-jerk control strategies minimize the longitudinal jerk to improve ride comfort. While the research on improving vehicle performance during lateral or vertical motion is very limited, and the early efforts by Hrovat and Hubbard [36,37] implemented an anti-jerk control strategy to enhance the ride comfort during vertical motion of a quarter car model. Where an augmented performance index is introduced to include the jerk rms term in addition to other outputs to improve the ride comfort, their results for one degree of freedom (DOF) quarter car model showed a reduction in rms jerk at the cost of an increase in rms of heaving acceleration, tire deflection, and rattle space. In [38], they further investigated the application of optimal anti-jerk controller for a two DOF quarter car model. They predicted a maximum reduction in rms jerk can be obtained at the cost of a modest increase of 23% in rattle space and a significant increase of 127 % in tire deflection. Hence, such significant improvement in ride quality can be achievable at the penalty of vehicle handling. In [39], using a semi-active suspension system we have implemented a preview-based anti-jerk control strategy to improve ride comfort without degrading the road-holding capability under different road conditions. Despite the exciting results to the researcher's knowledge, the previous anti-jerk methodologies only focus on enhancing ride comfort using conventional active or semi-active suspension systems. Moreover, the high speed of vehicles can also limit the application of these conventional methodologies. Therefore,

 doi:10.20944/preprints202305.0142.v1

in [40], we have implemented an active aerodynamic-based anti-jerk control strategy on a half-car model to improve the vehicle performance under different road conditions, i.e., bump input and asphalt road. However, load transfer effects during lateral motion are not considered, which greatly impacts passengers' ride comfort during cornering braking or forward acceleration.

Leaning the vehicle body against the vehicle body forces during lateral or longitudinal motion is very useful to mitigate the load transfer effects to enhance ride comfort. For example, in [41,42] used an anti-roll bar methodology to reduce the impact of load transfer during cornering. In [43,44], tilting control systems were developed to improve vehicle safety during cornering. In [45], we have designed a preview-based attitude controller to reduce the load transfer effect and track the desired roll and pitch position during cornering or forward acceleration to enhance ride quality. Similarly, in [6], using a conventional active suspension system, an attitude motion controller was developed for vehicles with active passenger seat systems to improve ride comfort and vehicle handling. In [20], we implemented an AAC strategy to tilt the vehicle body against centrifugal or inertial forces to track the desired roll or pitch position to enhance ride performance. But the main essential issue with aerodynamic surfaces is their abrupt moment which can cause discomfort to passengers. Therefore, it is important to achieve realistic motion of aerodynamic surfaces to reduce the vehicle body jerk during attitude motion.

Motivated by these perceptions, in this paper, four degrees of freedom half car equipped with aerodynamic surfaces is considered to explore the applications of the aerodynamic-based anti-jerk optimal control strategy, which is comprised of a feed-forward control strategy in addition to the state feedback controller. The feed-forward control can anticipate the force required to track the desired attitude angle. The state feedback controller can adjust the force to minimize error and jerk. Our main goal is to achieve realistic motion of aerodynamic surfaces to minimize vehicle body jerks. Anti-jerk optimal control with known predicted information regarding the future road maneuver is proposed to enhance the ride comfort during cornering, braking, or accelerating. The difference between braking and cornering is that the braking performance is dependent on the vehicle's speed only while cornering performance is dependent on the speed of the vehicle as well as the radius of curvature. The proposed optimal predictive control strategy can generate anticipating actions against future road maneuvers. Direct detection from sensors attached to the vehicle can provide information about future road maneuvers. The rest of the paper is organized as in section 2; the problem formulation is presented. Section 3 represents the proposed optimal anti-jerk control strategy, while section 4 discusses the simulation results, followed by a conclusion with future recommendations.

2. Problem Formulation

2.1. Vehicle Model

A schematic diagram of four degrees of freedom half-car model is shown in Figure 1, which can be considered as a longitudinal model in a forward direction or a lateral model during cornering. The proposed model is comprised of two unsprung masses and one sprung mass. The unsprung mass consists of masses m_1 and m_2, a damper with damping coefficients b_{s_1} and b_{s_2}, spring with stiffness coefficients k_{s_1} and k_{s_2}, and tire stiffness coefficients k_{t_1} and k_{t_2} at right and left side respectively. In contrast to conventional active suspension systems, two aerodynamic surfaces mounted on the sprung mass provide the necessary negative lift forces u_1 and u_2 to enhance ride comfort and road-holding capability. The hypothetical body forces f_1, f_2 acting on the vehicle body during cornering, braking, or forward acceleration. The parameter values of the addressed model are shown in Table 1. The mathematical model is derived using Newtonian methods. The equations of motion for the sprung mass acceleration and roll

Preprints (www.preprints.org) | NOT PEER-REVIEWED | Posted: 3 May 2023 doi:10.20944/preprints202305.0142.v1

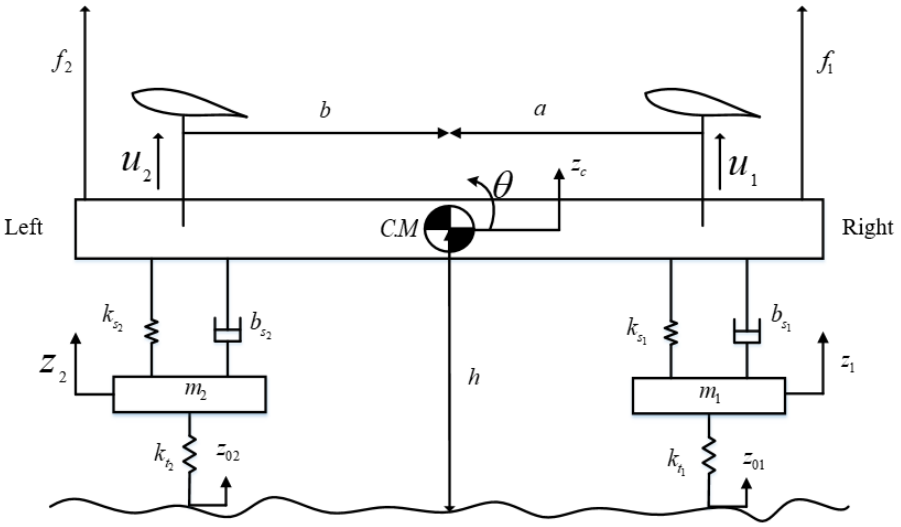

Figure 1. Four DOF lateral half-car model with active aerodynamic surfaces

Table 1: Parameter values of a four DOF half-car lateral and longitudinal model

Symbol	Lateral Model	Longitudinal Model	Unit
M	500	500	Kg
I	274	1222	Kgm^2
m_1, m_2	25	25	Kg
k_{s_1}, k_{s_2}	10	10	kN/m
k_{t_1}, k_{t_2}	1	1	kN/m
b_{s_1}, b_{s_2}	1	1	kN/m
a	0.74	1.25	m
b	0.74	1.1	m
h	0.70	0.70	m

or pitch angle are given as follows:

$$M\ddot{z}_c = f_l + f_r + u_1 + u_2 + f_1 + f_2 \tag{1}$$

$$I\ddot{\theta} = a(f_r + u_1 + f_1) - b(f_l + u_2 + f_2) \tag{2}$$

where Z_c sprung mass displacement, M is the sprung mass, θ is the attitude angle of the vehicle body, I is known as moment of inertia, f_r and f_l are right and left side suspension forces given in equations (3) and (4), respectively.

$$f_r = b_{s_1}(\dot{z}_1 - a\dot{\theta} - \dot{z}_c) + k_{s_1}(z_1 - a\theta - z_c) \tag{3}$$

$$f_l = b_{s_2}(\dot{z}_2 + b\dot{\theta} - \dot{z}_c) + k_{s_2}(z_2 + b\theta - z_c) \tag{4}$$

For the unsprung masses, the equations are given as:

$$m_1\ddot{z}_1 = -(k_{t_1}(z_1 - z_{01}) + f_r) \tag{5}$$

$$m_2\ddot{z}_2 = -(k_{t_2}(z_2 - z_{02}) + f_l) \tag{6}$$

The mounted suspension points on both sides experience two hypothetical disturbance

Preprints (www.preprints.org) | NOT PEER-REVIEWED | Posted: 3 May 2023 doi:10.20944/preprints202305.0142.v1

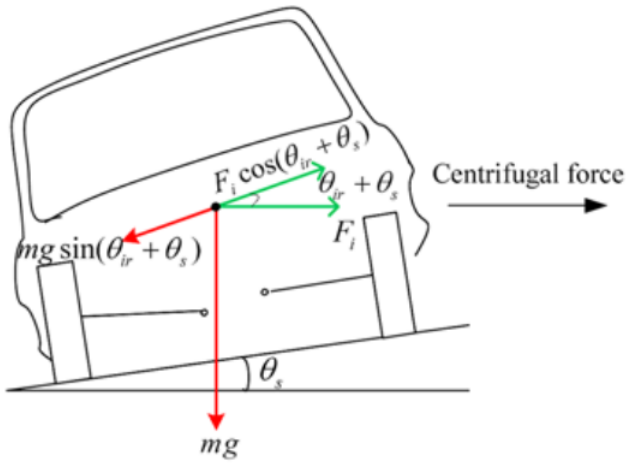

Figure 2. Schematic diagram for deriving the desired roll angle of a vehicle traveling with $120km/h$ speed during cornering.

forces, f_1 and f_2, with equal magnitudes but opposite directions. Equations (7) and (8) can be used to explain the forces acting on the body during the vehicle's roll and pitch motions, respectively. As shown in the following equations, namely, during roll motion, f_1 can be termed as f_{r_1} and f_2 is comparable to f_{r_2}, whereas, during pitch motion, f_1 is equal to f_{p_1} and f_2 is equal to f_{p_2}.

$$f_{r_{1,2}} = \left| F\cos(\theta_s) - \frac{mgh}{(a+b)}\sin(\theta_s) \right| \tag{7}$$

$$f_{p_{1,2}} = \left| F - \frac{mgh}{(a+b)}\sin(\theta_s) \right| \tag{8}$$

where the centrifugal or inertial force F occurs during cornering, vehicle acceleration, or braking. Additionally, g represents the gravitational force, and θ_s represents the slope of the road.

2.2. Desired Roll Angle

The schematic Figure 2 shows how to compute the desired roll position of the vehicle body during cornering.

$$mg\sin(\theta_s+\theta_{dr}) = ma_{ca}\cos(\theta_s+\theta_{dr}) \tag{9}$$

Rearranging the terms we get

$$\frac{a_{ca}}{g} = \frac{\tan(\theta_{dr})+\tan(\theta_s)}{1-\tan(\theta_s)\tan(\theta_{dr})} \tag{10}$$

θ_{dr} represents the desired roll angle which can be obtained as:

$$\theta_{dr} = \arctan\left(\frac{a_{ca}-g\tan(\theta_s)}{g+a_{ca}\tan(\theta_s)}\right) \tag{11}$$

where a_{ca} is called centrifugal acceleration.

2.3. Desired Pitch Angle

Figure 3 displays the optimal location for pitch on a sloped surface. When driving on a road with slope θ_s, it is preferable for the car's body to be parallel to the horizontal

Preprints (www.preprints.org) | NOT PEER-REVIEWED | Posted: 3 May 2023 doi:10.20944/preprints202305.0142.v1

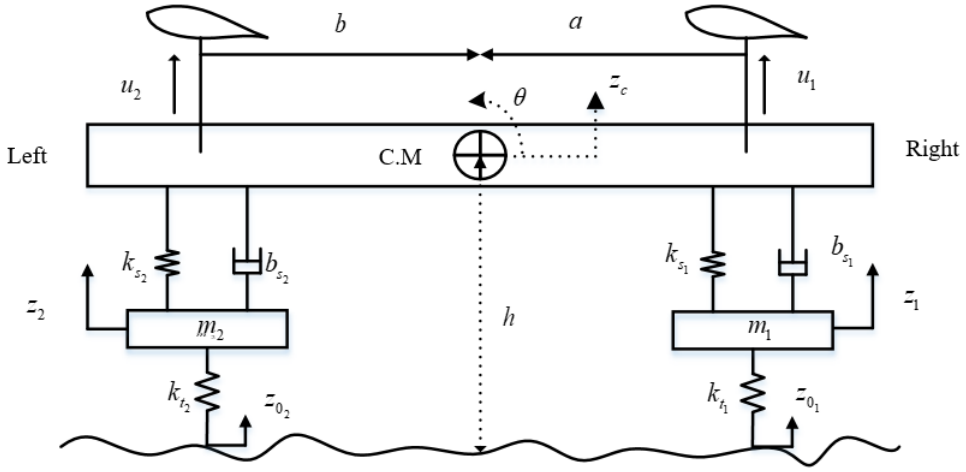

Figure 3. Schematic diagram for deriving the desired pitch angle of a vehicle traveling with $120km/h$ speed during acceleration or braking.

axis of the road. Equations (12) to (14) describe the calculation to determine the desired pitch angle.

$$mg\sin(\theta_s + \theta_{dp}) = ma_{ia}\cos(\theta_{dp}) \tag{12}$$

Rearranging the terms we get

$$\frac{a_{ia}}{g} = \tan(\theta_{dp})\cos(\theta_s) + \sin(\theta_s) \tag{13}$$

The desired pitch angle obtained is given as:

$$\theta_{dp} = \arctan\left(\frac{a_{ia}}{g\cos(\theta_s)}\right) - \theta_s \tag{14}$$

The roll angle θ_{dr} specified in equation (11) and the pitch angle θ_{dp} specified in equation (14) is calculated to counteract the external lateral and longitudinal forces that affect the passenger's ride comfort. Throughout the vehicle's motion, hypothetical body forces acting on both suspension mounting points have equal magnitudes and opposite directions. These forces are examined in the context of a car driving on a banked road, with particular attention paid to the magnitudes of hypothetical body forces during roll and pitch motions. To accomplish this, the jerk of control forces produced by the aerodynamic surfaces cancel out the derivative of these hypothetical body forces.

2.4. Aerodynamic Forces

This paper aims to improve a vehicle's ride performance using an active aerodynamic-based anti-jerk control strategy. By smoothly operating the aerodynamic surfaces, varying downward control forces can be produced, allowing the configuration of the AAS to deal with its distribution. This distribution significantly impacts the vehicle's ride performance, enabling adjustments to the sprung mass system vertical load to influence suspension deflection, vehicle body acceleration, and tire deflection. The AAS generate the necessary control forces are given as follows:

$$u_1 = \frac{1}{2}v^2\rho SC_{lift}(\alpha) \tag{15}$$

$$u_2 = \frac{1}{2}v^2\rho SC_{drag}(\alpha) \tag{16}$$

Preprints (www.preprints.org) | NOT PEER-REVIEWED | Posted: 3 May 2023 doi:10.20944/preprints202305.0142.v1

The lift coefficient C_{lift} and drag coefficient C_{drag} of the airfoil depend upon a number of variables, including the air density ρ, vehicle speed v, surface area S, angle of attack α, shape, and surface roughness. Differentiating equations (1) and (2) to obtain equations of heaving and angular jerk as given in (17) and (18) to design an anti-jerk controller with constantly known predicted information.

$$M\dddot{z}_c = \dot{f}_l + \dot{f}_r + \dot{u}_1 + \dot{u}_2 + \dot{f}_1 + \dot{f}_2 \tag{17}$$

$$I\ddot{\theta} = a(\dot{f}_r + \dot{u}_1) - b(\dot{f}_l + \dot{u}_2) + \dot{f}_1 + \dot{f}_2 \tag{18}$$

This study presents a novel anti-jerk predictive control approach designed to reduce the root-mean-square value of control jerk while enhancing the performance of aerodynamic surfaces. The optimal controller aims to minimize a cost function given in equation (19) consisting of heaving and angular acceleration, suspension and tire deflection, the difference between the actual and desired attitude angle, and jerk terms for the control inputs multiplied by weighting constants $\rho_1, \rho_2, \rho_3, \rho_4, \rho_5, \rho_7$, respectively. These weights establish the optimal distribution of the optimized criterion's various components.

$$\begin{aligned} J = \lim_{\tau\to\infty} \tfrac{1}{2T} \int_0^T (&\rho_1 \ddot{z_c}^2 + \rho_2 \ddot{\theta}^2 + \rho_3 (z_c + a\theta - z_1)^2 + \rho_3 (z_c - b\theta - z_2)^2 \\ &+ \rho_4 (\theta - \theta_d)^2 + \rho_5 (z_1 - z_{01})^2 + \rho_6 (z_2 - z_{02})^2 + \rho_7 \dot{u_1}^2 + \rho_7 \dot{u_2}^2) d\tau \end{aligned} \tag{19}$$

3. Optima Anti-jerk Controller Formulation

3.1. System Description

Continuous-time state-space model of the proposed half-car model can be represented as.

$$\dot{\mathbf{x}}(t) = \mathbf{A}\mathbf{x}(t) + \mathbf{B}\dot{\mathbf{u}}(t) + \mathbf{D}\mathbf{w}(t) \tag{20}$$

where $\mathbf{x}(t)$ represents the system's state vector,$\dot{\mathbf{u}}$ denotes the control jerk input, and $\mathbf{w}(t)$ is known as the disturbance jerk acting on the vehicle body.

$$\mathbf{x} = \begin{bmatrix} z_c & \dot{z}_c & \ddot{z}_c & \theta & \dot{\theta} & \ddot{\theta} & z_1 - z_{0_1} & \dot{z}_1 & z_2 - z_{0_2} & \dot{z}_2 & z_1 & z_2 \end{bmatrix}$$

$$\dot{\mathbf{u}} = \begin{bmatrix} \dot{u}_1 & \dot{u}_2 \end{bmatrix}^T, \dot{\mathbf{w}} = \begin{bmatrix} 0 & 0 & \dot{f}_1 & \dot{f}_2 \end{bmatrix}^T$$

$$\mathbf{x_d} = [0 \quad 0 \quad 0 \quad \theta_d \quad 0 \quad 0 \quad 0 \quad 0 \quad 0 \quad 0 \quad 0 \quad 0]$$

The constant matrices **A** and **B** have the appropriate dimensions as reported in our previous work [40]. The elements of the disturbance matrix **D** are given in Appendix A

3.2. Anti-jerk Controller Design

The performance index presented in equation (19) can be written in matrix form regarding the difference between the desired and current state, the jerk control inputs, and jerk disturbance inputs.

$$\begin{aligned} J = \lim_{\tau\to\infty} \tfrac{1}{2T} \int_0^T ((\mathbf{x} - \mathbf{x_d})^T Q (\mathbf{x} - \mathbf{x_d}) + 2(\mathbf{x} - \mathbf{x_d})^T N_2 \mathbf{w} + 2(\mathbf{x} - \mathbf{x_d})^T N_1 \dot{\mathbf{u}} \\ + \dot{\mathbf{u}}^T R \dot{\mathbf{u}} + 2\mathbf{w}^T M_1 \dot{\mathbf{u}} + \mathbf{w}^T M_2 \mathbf{w}) d\tau \end{aligned} \tag{21}$$

The Matrices Q, R, N_1, N_2, M_1, and M_2 refer to positive definite matrices as given in Appendix A. If the pair (A,B) is assumed to be stable and (A,Q) is detectable, then the anti-jerk controller can be derived by minimizing the performance index described in equation (21).

Preprints (www.preprints.org) | NOT PEER-REVIEWED | Posted: 3 May 2023 doi:10.20944/preprints202305.0142.v1

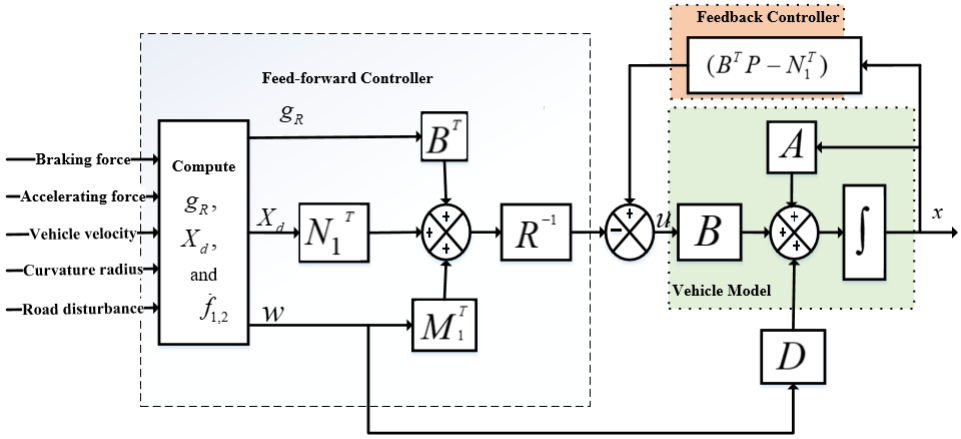

Figure 4. Block diagram consists of feed-forward to detect future road maneuvers and feedback controller to reduce the tracking error.

$$\dot{\mathbf{u}} = -R^{-1}((B^T P - N_1^T)\mathbf{x} + N_1^T \mathbf{x_d} + M_1^T \mathbf{w} + B^T \mathbf{g_R}) \tag{22}$$

where P is the solution of Algebraic Riccati Equation (ARE) given in equation (23).

$$0 = Q_n^T + A_n^T P + P A_n - P B R^{-1} B^T P \tag{23}$$

where

$$A_n = A + B R^{-1} N_1^T$$
$$Q_n = Q - N_1 R^{-1} N_1^T$$

The block diagram for the proposed anti-jerk control strategy is shown in Figure 4. The control strategy is composed of two parts, fee-forward part $B^T \mathbf{g_R}$ to provide an anticipated action against vehicle body jerks, and feedback part $-R^{-1}((B^T P - N_1^T)\mathbf{x} + N_1^T \mathbf{x_d}$ to reduce the tracking error between actual and desired attitude angle. The vector g_R satisfies

$$\mathbf{g_R} = \int_0^{tp} e^{-Ac^T \tau}((PD_n - N_n)\mathbf{w}(\tau) - (Q_n + PBR^{-1}N_1^T)\mathbf{x_d}(\tau))d\tau \tag{24}$$

where $D_n = D - BR^{-1}M_1^T$, $N_n = N_2 - N_1 R^{-1} M_1^T$, and $A_c = A_n - BR^{-1}B^T P$ is called asymptotically closed-loop stable matrix. The closed system equation can be obtained by putting equation (22) in (20) as given in (25):

$$\dot{x} = A_c x + D_n \mathbf{w} - BR^{-1} N T^1 \mathbf{x_d} - BR^{-1} B^T \mathbf{g_R} \tag{25}$$

4. Simulation Results and Discussion

In this section, the simulation result are discussed, which are conducted using MATLAB 2022b installed on a Samsung Core™ 5-6400 CPU @ 2.70 GHz to perform simulations of a vehicle's attitude motions while traveling at a speed of 120 km/hr. The different scenarios are considered to investigate the effectiveness of the proposed anti-jerk predictive control strategy (AJPC). In the first case, the simulations are conducted for lane-change maneuvers to evaluate the performance of the proposed AJPC to track the desired roll angle and improve ride comfort and road-holding capability. For the second case, pitch motion simulations are performed during braking and accelerating the vehicle to analyze the proposed control strategy's impact on minimizing oscillations in the vehicle body's vertical motion and tire deflection. The control strategy successfully

 doi:10.20944/preprints202305.0142.v1

mitigated the external centrifugal and longitudinal jerks acting on the vehicle body and helped to achieve the desired attitude motion. Comparing the performance of anti-jerk predictive control and predictive control (PC) without jerk using the root mean square error (RMSE) method, the AJPC outperformed the PC without jerk in terms of ride comfort and road-holding capability. The findings imply that prioritizing high weighting for control jerk can have a detrimental effect on vehicle performance. Although the impact on desired attitude angle tracking is minor and unlikely to affect overall vehicle performance significantly, it is worth noting that the objective of this research is not only to enhance both ride comfort and vehicle handling simultaneously but also to achieve more realistic operation of aerodynamic surfaces.

4.1. Roll Angle Tracking

This section presents simulation results for a half-car model equipped with aerodynamic surfaces, traveling at a constant speed of 120 km/h during a double-lane change maneuver. The performance of the proposed AJPC is investigated in the presence of centrifugal jerks acting on the vehicle body during a double lane change maneuver. Figure 5 illustrates the simulation results for the desired roll angle tracking of the vehicle, which show that the tracking performance of the proposed AJPC is slower than that of the PC without jerk, mainly due to the slower motion of the aerodynamic surfaces, as shown in Figure 9. The simulation results for the vehicle body jerk are shown in Figure 6, which shows the proposed control strategy successfully reduces the heaving and rolling jerks during cornering. This can also be verified from Table 2, where compared to the predictive control, the proposed AJPC reduces the heaving jerk by 18% and the rolling jerk by 21%. Hence confirms an improvement in ride comfort. Figure 7 shows the heaving and roll acceleration simulation results. The proposed AJPC strategy resulted in lower heaving and roll acceleration than the PC strategy without jerk. Table 2 further highlights that the proposed AJPC strategy reduced heaving acceleration by 14% and rolling acceleration by 27%, thus enhancing ride comfort. Figure 8 shows the tire and suspension deflection simulation results. The results indicate that the tire deflection causes high overshoots for PC without jerk, weakening the tire's grip on the road while turning on a double lane-change maneuver. Table 2 indicates 7% enhancement in road holding capability for the proposed AJPC strategy. Figure 9 shows the results for the jerk control input, where the controlling jerk for the proposed AJPC has minimum overshoots, confirming that the smooth and realistic operation of the aerodynamic surfaces has a great impact on the vehicle's ride performance. Therefore, the proposed AJPC strategy improved ride comfort while maintaining the aerodynamic surfaces' realistic motion at the cost of slower desired attitude motion tracking.

Table 2: Root mean square error (RMSE) values for roll motion.

Parameter	PC without jerk	AJPC
Heaving jerk	100	82.11
Roll jerk	100	79.23
Jerk controller	100	40.25
Heaving acceleration	100	86.38
Roll acceleration	100	73.12
Tyre deflection	100	92.67
Suspension deflection	100	99.83

Preprints (www.preprints.org) | NOT PEER-REVIEWED | Posted: 3 May 2023 doi:10.20944/preprints202305.0142.v1

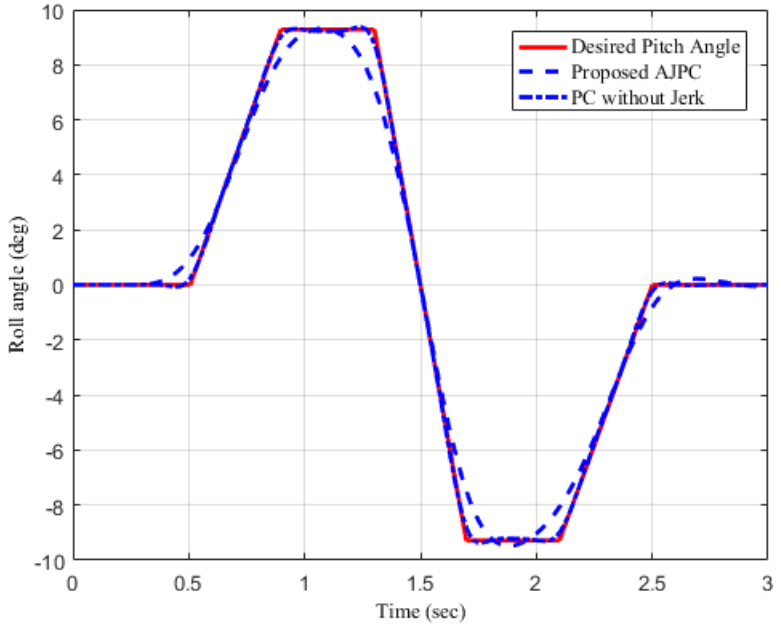

Figure 5. Desired roll angle tracking of a half-car traveling on a double lane change maneuver with $120km/h$

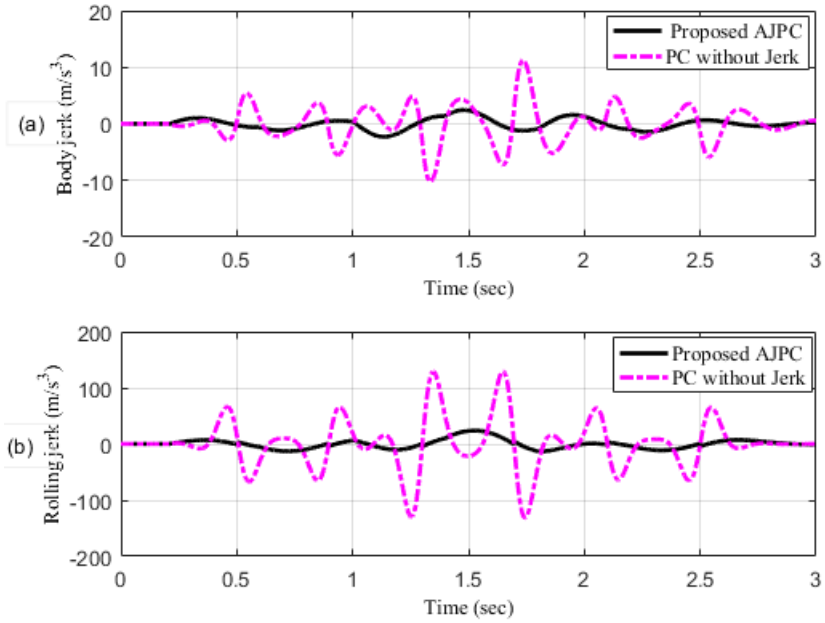

Figure 6. Heaving and rolling jerk of a half-car traveling on a double lane change maneuver with $120km/h$ (a) Heaving jerk (b) Rolling jerk

Preprints (www.preprints.org) | NOT PEER-REVIEWED | Posted: 3 May 2023 doi:10.20944/preprints202305.0142.v1

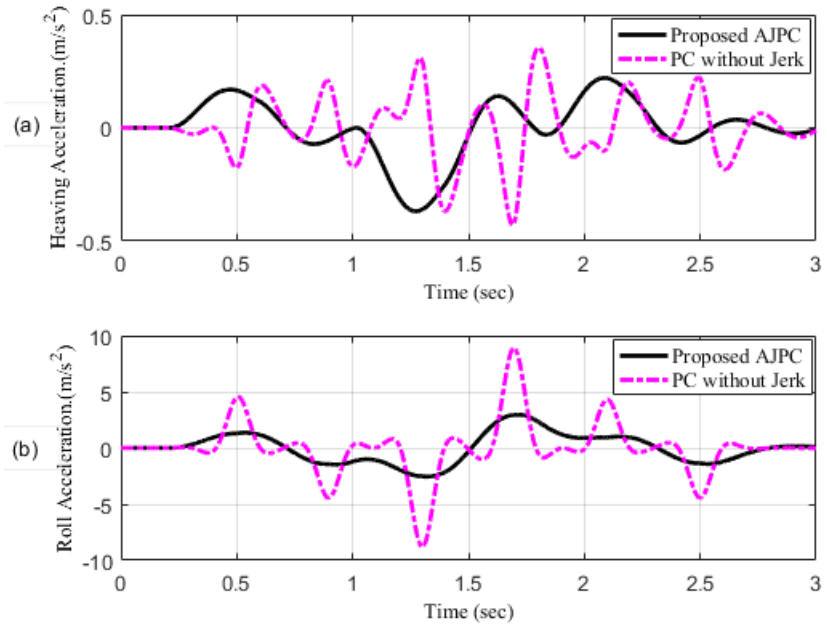

Figure 7. Heaving and rolling acceleration of a half-car traveling on a double lane change maneuver with 120km/h (a) Heaving acceleration (b) Rolling acceleration

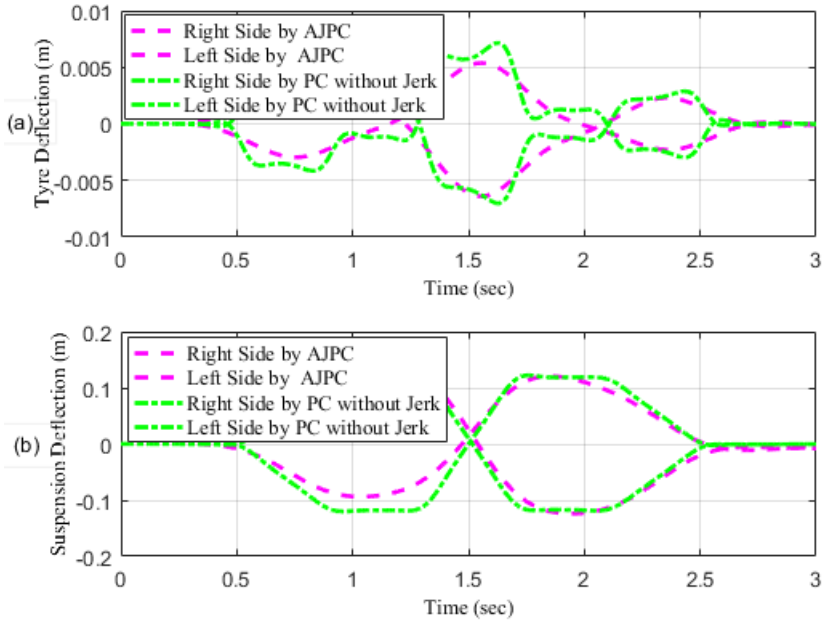

Figure 8. Tire and suspension deflection of half-car traveling on a double lane change maneuver with 120km/h (a) Tire deflection (b) Suspension deflection

Preprints (www.preprints.org) | NOT PEER-REVIEWED | Posted: 3 May 2023 doi:10.20944/preprints202305.0142.v1

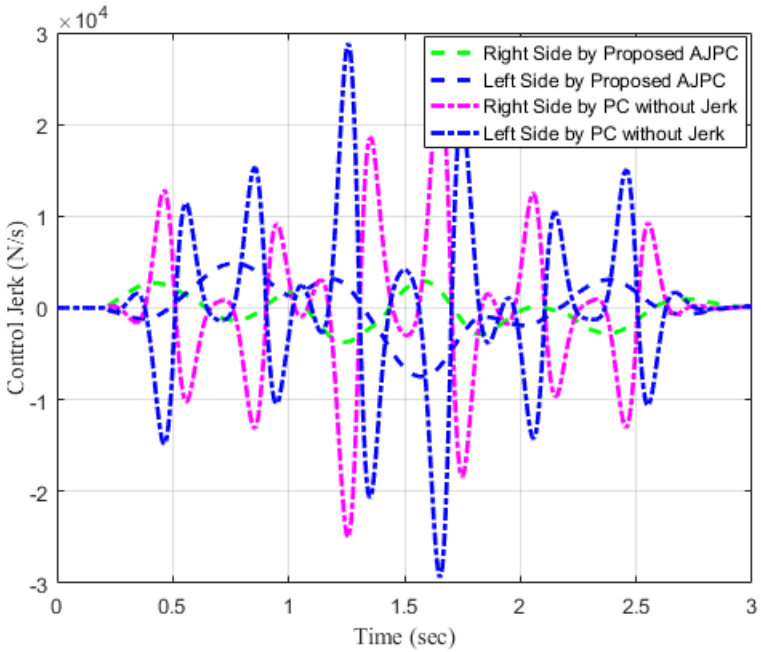

Figure 9. Control jerk of a vehicle traveling on a double lane change maneuver with $120km/h$

4.2. Desired Pitch Angle Tracking

In this section, the simulation results are carried out for the half-car model when traveling with $120km/h$ considering two different cases. In the first case, the simulations are performed while accelerating the vehicle in the forward direction. The accelerating force will generate inertial forces to produce a backward pitch motion, resulting in discomfort to the passenger. The optimal solution is to adjust the vehicle's forward pitch to cancel the inertial effects that occur while accelerating the vehicle. This will make passengers feel comfortable, with the ideal pitch angle being zero. Figure 10 displays the simulation results for desired pitch angle tracking, demonstrating that compared to the anti-jerk predictive control strategy, the predictive control strategy exhibits outstanding performance in tracking the desired pitch motion. The poor tracking by the proposed AJPC strategy is due to the realistic slower motion of the aerodynamic surfaces as shown in Figure 14. However, the operation of the aerodynamic surfaces is very effective in improving the vehicle's ride quality. For example, as shown in Figure 11, both the heaving and pitching jerks are reduced in the case of AJPC, which shows that compared to PC without jerk, the proposed AJPC strategy successfully improves the ride comfort. Similarly, comparing the rms values in Table 3 indicates that the proposed AJPC strategy has a 16% lower heaving and 9% pitching jerk. The reduction in the rms values validates a significant improvement in ride comfort. Similarly, Figure 12 shows the simulation results for heaving and pitching accelerations. This indicates that compared to the PC without jerk, the proposed control strategy has lower heaving and pitching acceleration. This can be verified from Table 3. Figure 13 shows the simulation results for tire and suspension deflection, which shows that while improving the ride comfort, the tire's grip on the road is not degraded for the AJPC strategy. Table 3 also shows that both tire and suspension deflection for the proposed AJPC strategy and PC strategy is almost identical. Hence we can conclude that using high weights for the control jerk inputs can successfully improve ride comfort without degrading road-holding capability at the cost of slow attitude motion tracking.

 doi:10.20944/preprints202305.0142.v1

Table 3: Root mean square error (RMSE) values for pitch motion during accelerating.

Parameter	PC without jerk	AJPC
Heaving jerk	100	84.10
Pitching jerk	100	91.31
Jerk controller	100	63.32
Heaving Acceleration	100	85.80
Pitching Acceleration	100	93.78
Tyre deflection	100	99
Suspension deflection	100	100

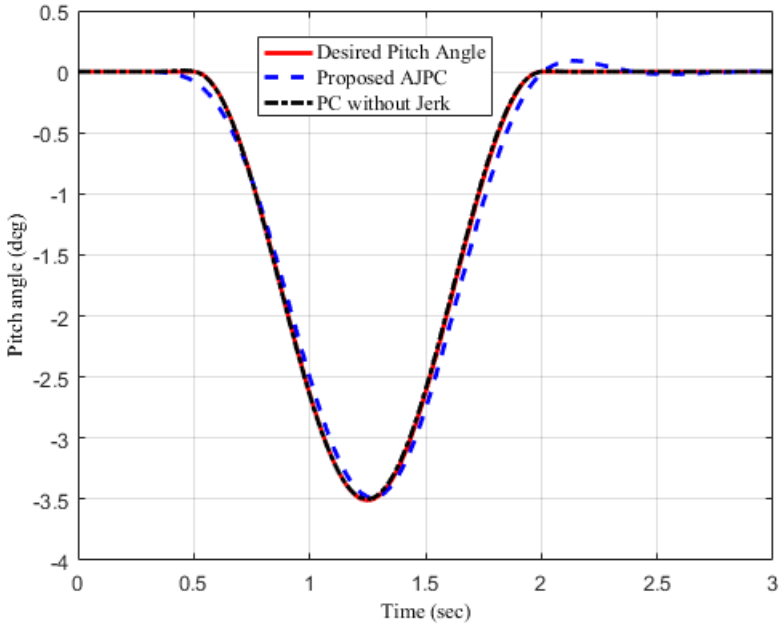

Figure 10. Simulation results for desired pitch angle tracking of a half-car during acceleration

Preprints (www.preprints.org) | NOT PEER-REVIEWED | Posted: 3 May 2023 doi:10.20944/preprints202305.0142.v1

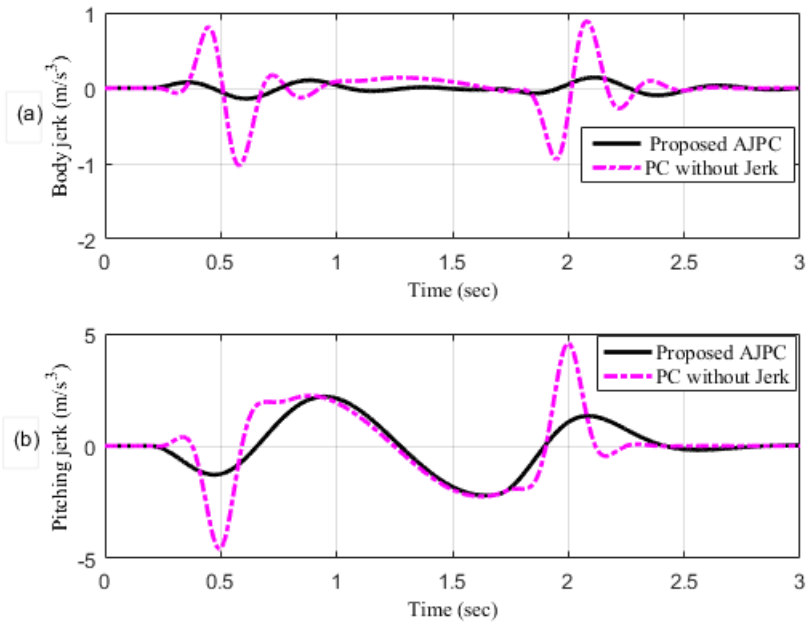

Figure 11. Simulation results heaving and pitching jerk of a half-car during acceleration (a) Heaving acceleration (b) Pitching acceleration

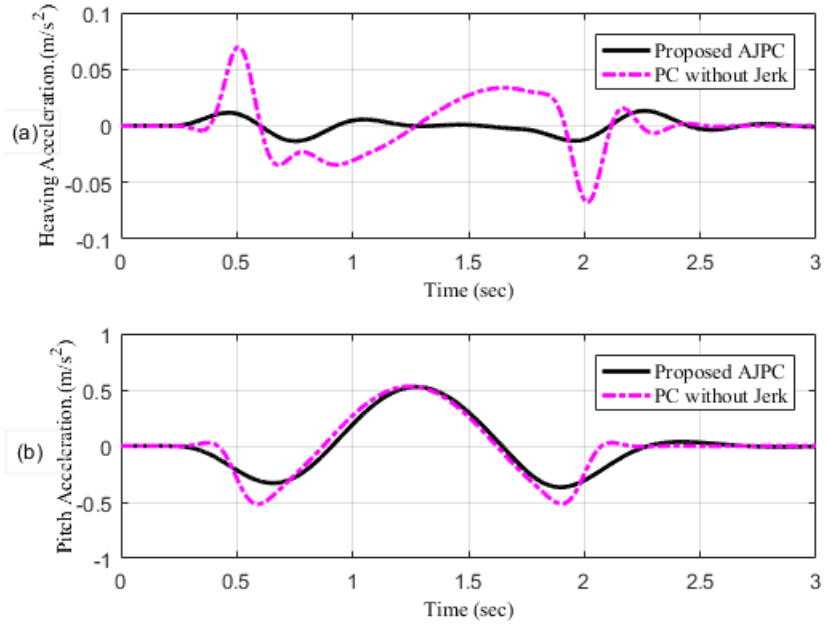

Figure 12. Simulation results heaving and Pitching acceleration of a half-car during acceleration (a) Heaving acceleration (b) Pitching acceleration

Preprints (www.preprints.org) | NOT PEER-REVIEWED | Posted: 3 May 2023 doi:10.20944/preprints202305.0142.v1

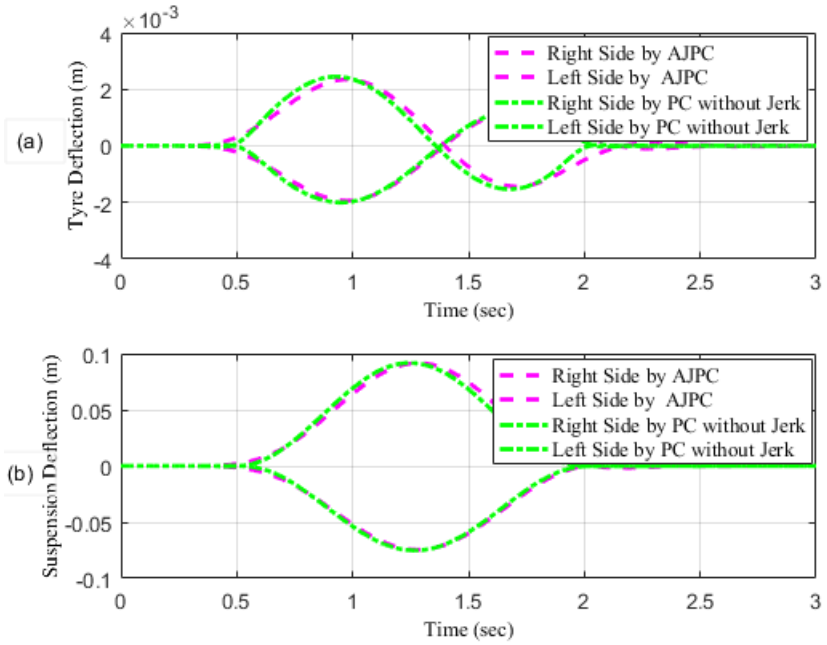

Figure 13. Simulation results for tire and suspension deflection of a half-car during acceleration (a) Tire deflection (b) Suspension deflection

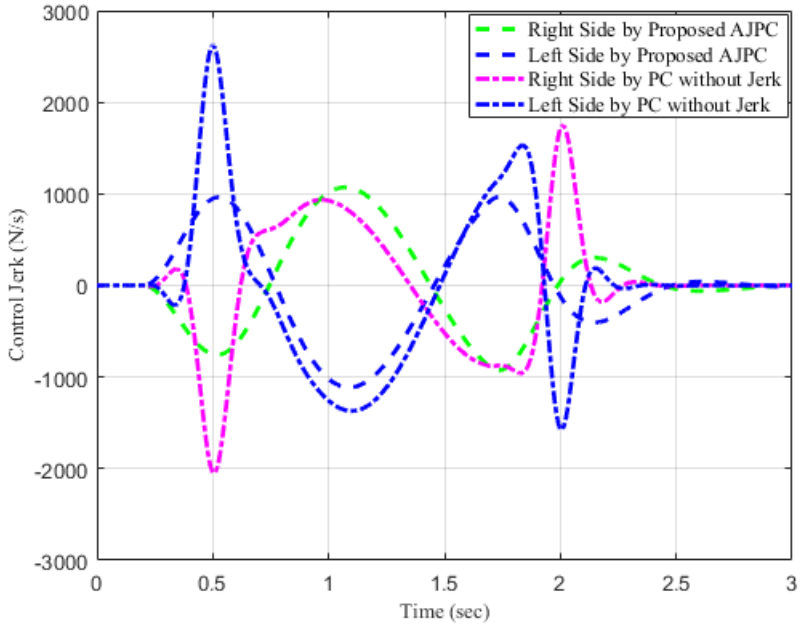

Figure 14. Simulation results for control jerk of a vehicle during acceleration

For the second case, the simulation results are carried out for the half-car model while braking when traveling on a sloped road. During braking, the braking force will generate inertial forces to produce a forward-pitch motion that can cause the passenger discomfort. The optimal solution is to adjust the vehicle's backward pitch to cancel out the inertial effects that occur while braking. This will allow passengers to feel comfortable with the ideal backward pitch angle. Figure 15 displays the simulation results for desired pitch angle tracking, which show that when compared to the anti-jerk predictive control approach, the predictive control technique displays remarkable performance in tracking the appropriate pitch motion during braking. The realistically

Preprints (www.preprints.org) | NOT PEER-REVIEWED | Posted: 3 May 2023 doi:10.20944/preprints202305.0142.v1

slower motion of the aerodynamic surfaces leads to the poor tracking of the suggested AJPC approach, as shown in Figure 19. However, using aerodynamic surfaces effectively can significantly enhance a vehicle's ride quality. Figure 16 shows the simulation results for heaving and pitching jerks, indicating that the proposed AJPC successfully reduces these jerks to improve ride comfort. Comparing the rms values in Table 3 shows that the proposed AJPC approach has a 12% lower heaving jerk and a 3 % lower pitching jerk. Figure 17 shows the heaving and pitching acceleration results while braking the vehicle. The results indicate that compared to the PC without jerk, the heaving acceleration for the AJPC is 11% lowered, and pitching acceleration is 13% lowered. This confirms an improvement in ride comfort. The simulation results for tire and suspension deflection are shown in Figure 18, demonstrating that while the AJPC method enhances ride comfort, the tire's grip on the road is not compromised. Thus, we can conclude that the proposed AJPC successfully improves ride performance at the cost of poor pitch motion tracking.

Table 4: Root mean square error (RMSE) values for pitch motion during braking.

Parameter	PC without jerk	AJPC
Heaving jerk	100	88.40
Pitching jerk	100	85.14
Jerk controller	100	45.11
Heaving Acceleration	100	89.72
Pitching Acceleration	100	87.78
Tyre deflection	100	98.54
Suspension deflection	100	90.32

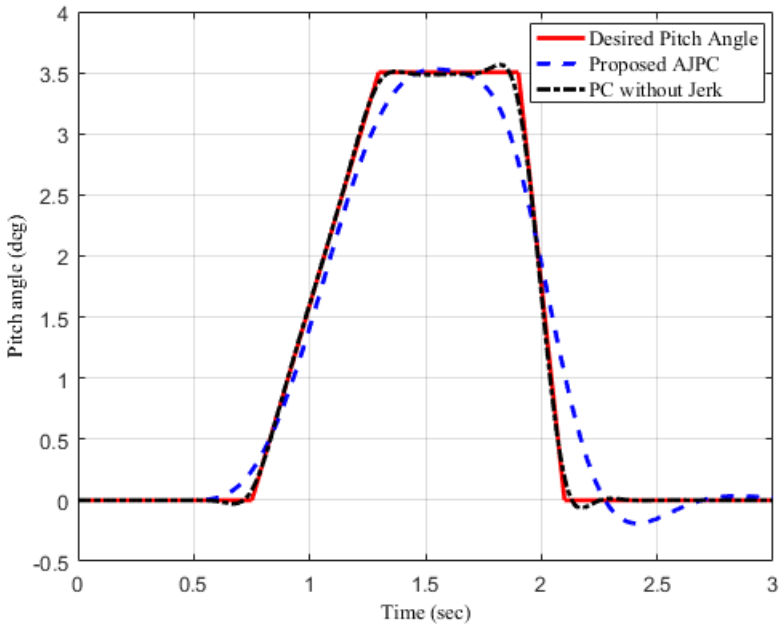

Figure 15. Desired pitch angle tracking of a half-car during braking

Preprints (www.preprints.org) | NOT PEER-REVIEWED | Posted: 3 May 2023 doi:10.20944/preprints202305.0142.v1

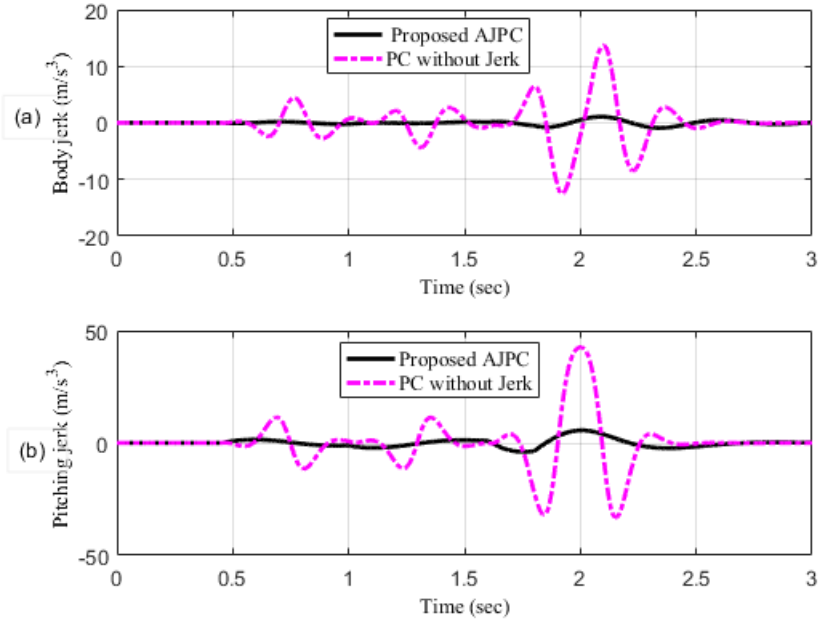

Figure 16. Simulation results for heaving and pitching jerks of a half-car during braking (a) Heaving jerk (b) Pitching jerk

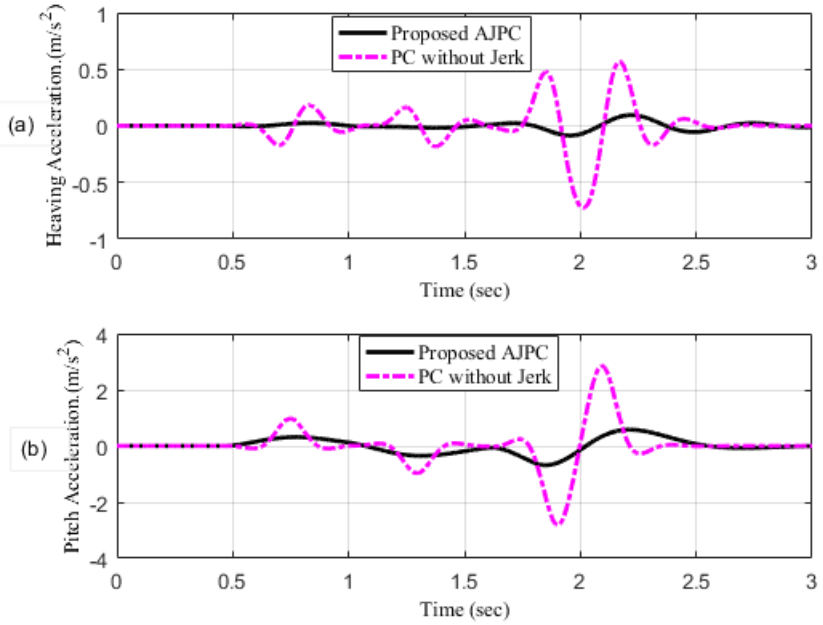

Figure 17. Simulation results for heaving and pitching accelerations of a half-car during braking (a) Heaving acceleration (b) Pitching acceleration

Preprints (www.preprints.org) | NOT PEER-REVIEWED | Posted: 3 May 2023 doi:10.20944/preprints202305.0142.v1

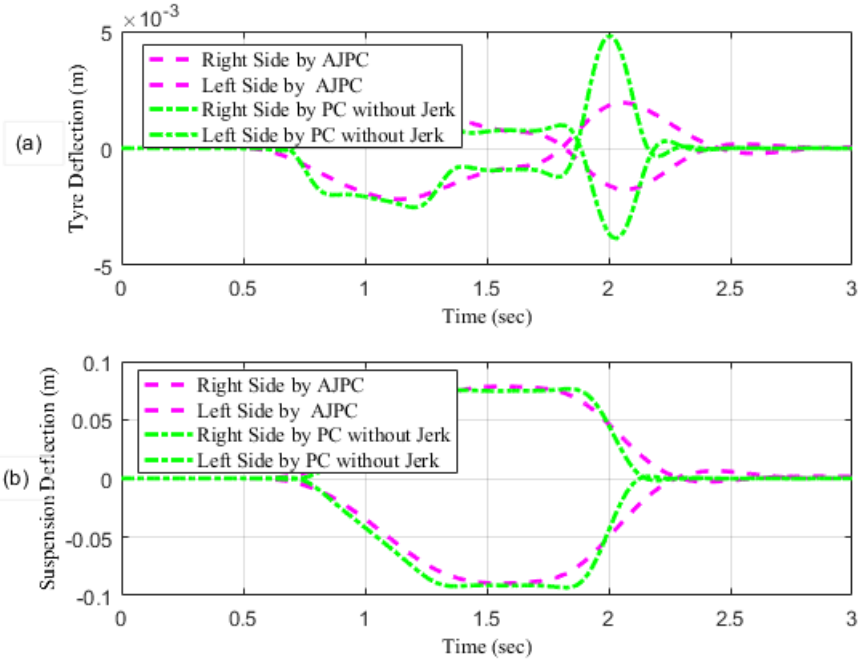

Figure 18. Simulation results for tire and suspension deflection of a half-car during braking (a) Tire deflection (b) Suspension deflection

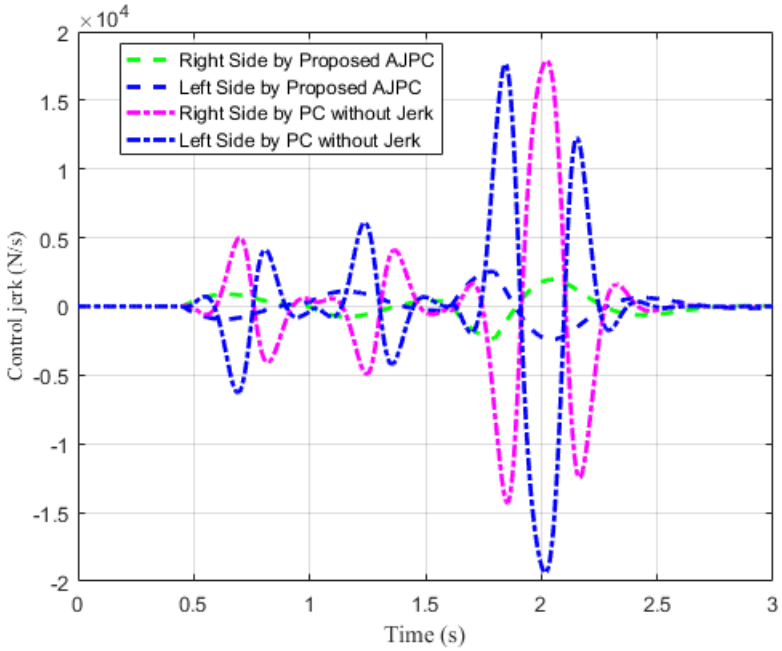

Figure 19. Simulation results for control jerk of a vehicle during braking

The implementation of the proposed strategy raises a question about whether to use a force control or a discrete-time implementation of its derivative, given the availability of a force actuator. While a force control approach may be preferred, a discrete-time implementation using the difference in actuator force Δu over discrete time intervals is also feasible. One advantage of the discrete-time implementation is that the output force will remain unchanged if the computer fails, avoiding the potential for an undesired force output. Instead, it will maintain the previous force value.

 doi:10.20944/preprints202305.0142.v1

5. Conclusion

The anti-jerk predictive control technique proposed in this research is investigated to enhance the ride performance of vehicles during attitude motion while cornering, accelerating, and braking. The proposed method improved the ride comfort and road-holding ability of the vehicle fitted with active aerodynamic surfaces by canceling the centrifugal jerks during cornering and inertial jerks during acceleration and braking. The anti-jerk controller comprises two parts: a feed-forward component that uses the future road maneuver and a feedback component to address tracking errors made up of the control approach. The proposed control technique successfully achieved the realistic motion of the AAS to reduce the vehicle body jerk during attitude motion. The simulation results demonstrate that the suggested technique successfully reduced control jerk to improve AAS performance and reduced heaving, rolling, or pitching jerk and acceleration to improve ride comfort without compromising road holding capability. The results further validate that the anti-jerk predictive controller enhanced the half car's ride comfort and stability and significantly lessened the effect of the hypothetical body jerks. The following future recommendations can be taken into account to explore the applications of the proposed approach.

- The current work can be extended to a full car model along with the actuator dynamics of the airfoil.
- The discrete-time implementation of the suggested control method will allow future research into the proposed control strategy.
- Robust and intelligent control algorithms may be considered to address both air and road disturbances.

Acknowledgment

This work is supported by the Gyeongsang National University, Jinju, South Korea.

Appendix A

The non-zero entries for matrix **D** are

$$d_{33} = d_{34} = 1/M$$
$$d_{63} = a/I, d_{64} = -b/I$$

The elements of weight matrix **Q** defined in (21) are given as follows

$$q_{ij} = \begin{cases} \rho_1 a_{3i} a_{3j} + \rho_2 a_{6i} a_{6j} & \text{if} \quad i \neq j \\ \psi_{ij} & \text{if} \quad i = j \end{cases}$$

with special entries as:

$$\psi_{11} = \rho_1 a_{31} a_{31} + \rho_2 a_{61} a_{61} + \rho_3,$$
$$\psi_{33} = \rho_1 a_{33} a_{33} + \rho_2 a_{63} a_{63} + \rho_1,$$
$$\psi_{44} = \rho_1 a_{34} a_{34} + \rho_2 a_{64} a_{64} + a\rho_3 - b\rho_3 + \rho_4,$$
$$\psi_{66} = \rho_1 a_{66} a_{66} + \rho_2 a_{66} a_{66} + \rho_2,$$
$$\psi_{77} = \rho_1 a_{37} a_{37} + \rho_2 a_{67} a_{67} + \rho_5,$$
$$\psi_{99} = \rho_1 a_{39} a_{39} + \rho_2 a_{69} a_{69} + \rho_5,$$
$$\psi_{1010} = \rho_1 a_{310} a_{310} + \rho_2 a_{610} a_{610},$$
$$\psi_{1111} = \rho_1 a_{311} a_{311} + \rho_2 a_{611} a_{611} + \rho_3,$$
$$\psi_{1212} = \rho_1 a_{312} a_{312} + \rho_2 a_{612} a_{612} + \rho_3$$

Non zero elements of Matrices $\mathbf{N_1}, \mathbf{N_2}, \mathbf{M_1}$ and M_2 are given as follows:

$$
\begin{aligned}
n_{1ij} &= \rho_1 a_{3i} b_{3j} + \rho_2 a_{6i} b_{6j} \quad i = 1,..,12, \quad j = 1,2 \\
n_{2ij} &= \rho_1 a_{3i} d_{3j} + \rho_2 a_{6i} d_{6j} \quad i = 1,..,12, \quad j = 1,2 \\
m_{1ij} &= \rho_1 d_{7i} b_{3j} + \rho_2 d_{9i} b_{6j} \quad i = 1, \quad j = 1,2 \\
m_{2ij} &= \rho_1 d_{7i} b_{3j} + \rho_2 d_{9i} b_{6j} \quad i,j = 1,2
\end{aligned}
$$

References

1. He, D.; He, W.; Song, X. Efficient predictive cruise control of autonomous vehicles with improving ride comfort and safety. *Measurement and control* **2020**, *53*, 18–28.
2. Cvok, I.; Hrgetić, M.; Hoić, M.; Deur, J.; Ivanovic, V. Design of a linear motor-based shaker rig for testing driver's perceived ride comfort. *Mechatronics* **2021**, *75*, 102521.
3. Mata-Carballeira, Ó.; del Campo, I.; Asua, E. An eco-driving approach for ride comfort improvement. *IET Intelligent Transport Systems* **2022**, *16*, 186–205.
4. Tang, X.; Duan, Z.; Hu, X.; Pu, H.; Cao, D.; Lin, X. Improving ride comfort and fuel economy of connected hybrid electric vehicles based on traffic signals and real road information. *IEEE Transactions on Vehicular Technology* **2021**, *70*, 3101–3112.
5. Ahmad, E.; Song, Y.; Khan, M.A.; Youn, I. Attitude Motion Control of a Half car Model with Tracking Controller Using Aerodynamic Surfaces. 2019 International Automatic Control Conference (CACS). IEEE, 2019, pp. 1–6.
6. Liang, W.; Khan, M.A.; Youn, E.; Youn, I.; Tomizuka, M. Attitude motion control of vehicle including the active passenger seat system. *International Journal of Vehicle Design* **2018**, *78*, 131–160.
7. Sadeghi, J.; Rabiee, S.; Khajehdezfuly, A. Effect of rail irregularities on ride comfort of train moving over ballast-less tracks. *International Journal of Structural Stability and Dynamics* **2019**, *19*, 1950060.
8. Savkoor, A.; Manders, S.; Riva, P. Design of actively controlled aerodynamic devices for reducing pitch and heave of truck cabins. *JSAE review* **2001**, *22*, 421–434.
9. Savkoor, A. Aerodynamic vehicle ride control with active spoilers. *Proc. AVEC'96* **1996**, pp. 647–681.
10. Meijaard, J.; Savkoor, A.; Lodewijks, G. Potential for vehicle ride improvement using both suspension and aerodynamic actuators. Proceedings of the IEEE International Symposium on Industrial Electronics, 2005. ISIE 2005. IEEE, 2005, Vol. 1, pp. 385–390.
11. Doniselli, C.; Mastinu, G.; Gobbi, M. Aerodynamic effects on ride comfort and road holding of automobiles. *Vehicle System Dynamics* **1996**, *25*, 99–125.
12. Corno, M.; Bottelli, S.; Panzani, G.; Spelta, C.; Tanelli, M.; Savaresi, S.M. Performance assessment of active aerodynamic surfaces for comfort and handling optimization in sport cars. *IEEE Transactions on Control Systems Technology* **2015**, *24*, 189–199.
13. Hosseinian Ahangarnejad, A.; Melzi, S. Numerical analysis of the influence of an actively controlled spoiler on the handling of a sports car. *Journal of Vibration and Control* **2018**, *24*, 5437–5448.
14. Diba, F.; Barari, A.; Esmailzadeh, E. Handling and safety enhancement of race cars using active aerodynamic systems. *Vehicle system dynamics* **2014**, *52*, 1171–1190.
15. Diba, F.; Barari, A.; Esmailzadeh, E. Active Aerodynamic System to Improve the Safety and Handling of Race Cars in Lane Change and Wet Road Maneuvers. International Design Engineering Technical Conferences and Computers and Information in Engineering Conference. American Society of Mechanical Engineers, 2012, Vol. 45059, pp. 417–423.
16. Wu, Y.; Chen, Z. Improving Road Holding and Ride Comfort of Vehicle Using Dual Active Aerodynamic Surfaces. 2018 2nd International Conference on Robotics and Automation Sciences (ICRAS). IEEE, 2018, pp. 1–5.
17. Hammad, M.; Qureshi, K.; He, Y. Safety and lateral dynamics improvement of a race car using active rear wing control. Technical report, SAE Technical Paper, 2019.
18. Ayyagari, D.T.; He, Y. Aerodynamic analysis of an active rear split spoiler for improving lateral stability of high-speed vehicles. *International Journal of Vehicle Systems Modelling and Testing* **2017**, *12*, 217–239.
19. Zhang, X.; Toet, W.; Zerihan, J. Ground effect aerodynamics of race cars **2006**.
20. Ahmad, E.; Iqbal, J.; Arshad Khan, M.; Liang, W.; Youn, I. Predictive Control Using Active Aerodynamic Surfaces to Improve Ride Quality of a Vehicle. *Electronics* **2020**, *9*, 1463.
21. Grant, P.R.; Haycock, B. Effect of jerk and acceleration on the perception of motion strength. *Journal of Aircraft* **2008**, *45*, 1190–1197.
22. Pendrill, A.M.; Eager, D. Velocity, acceleration, jerk, snap and vibration: Forces in our bodies during a roller coaster ride. *Physics Education* **2020**, *55*, 065012.
23. Sicat, S.; Woodcock, K.; Ferworn, A. Wearable technology for design and safety evaluation of rider acceleration exposure on aerial adventure attractions. Proceedings of the Annual Occupational Ergonomics and Safety Conference, Pittsburgh, PA, USA, 2018, pp. 7–8.
24. Gierlak, P.; Szybicki, D.; Kurc, K.; Burghardt, A.; Wydrzyński, D.; Sitek, R.; Goczał, M. Design and dynamic testing of a roller coaster running wheel with a passive vibration damping system. *Journal of Vibroengineering* **2018**, *20*, 1129–1143.

25. Nemes, A.; Mester, G. Energy Efficient Feasible Autonomous Multi-Rotor Unmanned Aerial Vehicles Trajectories. Proceedings of the 4th International Scientific Conference on Advances in Mechanical Engineering, ISCAME, 2016, pp. 369–376.
26. Werkman, J. Determining and predicting the seakeeping performance of ships based on jerk in the ship motions **2019**.
27. Bae, I.; Moon, J.; Seo, J. Toward a comfortable driving experience for a self-driving shuttle bus. *Electronics* **2019**, *8*, 943.
28. Scamarcio, A.; Metzler, M.; Gruber, P.; De Pinto, S.; Sorniotti, A. Comparison of anti-jerk controllers for electric vehicles with on-board motors. *IEEE Transactions on Vehicular Technology* **2020**, *69*, 10681–10699.
29. Scamarcio, A.; Gruber, P.; De Pinto, S.; Sorniotti, A. Anti-jerk controllers for automotive applications: A review. *Annual Reviews in Control* **2020**, *50*, 174–189.
30. Batra, M.; Maitland, A.; McPhee, J.; Azad, N.L. Non-linear model predictive anti-jerk cruise control for electric vehicles with slip-based constraints. 2018 annual American control conference (ACC). IEEE, 2018, pp. 3915–3920.
31. Noceda, J.C. Model Predictive Anti-Jerk Control of an Electrified Drivetrain with Backlash. PhD thesis, 2023.
32. Jing, J.; Liu, Y.; Wu, J.; Huang, W.; Zuo, B.; Yang, G. Research on drivability control in P2. 5 hybrid system. *Energy Reports* **2021**, *7*, 1582–1593.
33. Yue, Y.; Huang, Y.; Hao, D.; Zhu, G.G. Model reference adaptive LQT control for anti-jerk utilizing tire-road interaction characteristics. *Proceedings of the Institution of Mechanical Engineers, Part D: Journal of Automobile Engineering* **2021**, *235*, 1670–1684.
34. Liu, Y.; Zuo, L. Mixed skyhook and power-driven-damper: A new low-jerk semi-active suspension control based on power flow analysis. *Journal of Dynamic Systems, Measurement, and Control* **2016**, *138*.
35. Yamaguchi, A.; Ohishi, K.; Yokokura, Y.; Miyazaki, T.; Sasazaki, K. Backlash-based Shock Isolation Control for Jerk Reduction in Clutch Engagement. *IEEJ Journal of Industry Applications* **2019**, *8*, 160–169.
36. Hrovat, D.; Hubbard, M. Optimum vehicle suspensions minimizing rms rattlespace, sprung-mass acceleration and jerk **1981**.
37. Hrovat, D.; Hubbard, M. A comparison between jerk optimal and acceleration optimal vibration isolation. *Journal of Sound and Vibration* **1987**, *112*, 201–210.
38. Rutledge, D.; Hubbard, M.; Hrovat, D. A two DOF model for jerk optimal vehicle suspensions. *Vehicle System Dynamics* **1996**, *25*, 113–136.
39. Youn, I.; Ahmad, E. Anti-jerk optimal preview control strategy to enhance performance of active and semi-active suspension systems. *Electronics* **2022**, *11*, 1657.
40. Ahmad, E.; Youn, I. Performance Improvement of a Vehicle Equipped with Active Aerodynamic Surfaces Using Anti-Jerk Preview Control Strategy. *Sensors* **2022**, *22*, 8057.
41. Kelkar, S.S.; Gautam, P.; Sahai, S.; Agrawal, P.S.; Manoharan, R. A detailed study on design, fabrication, analysis, and testing of the anti-roll bar system for formula student cars. *SN Applied Sciences* **2021**, *3*, 1–14.
42. Chen, Y.; Peterson, A.W.; Ahmadian, M. Achieving anti-roll bar effect through air management in commercial vehicle pneumatic suspensions. *Vehicle system dynamics* **2019**, *57*, 1775–1794.
43. Karamuk, M.; Alankus, O.B. Development and Experimental Implementation of Active Tilt Control System Using a Servo Motor Actuator for Narrow Tilting Electric Vehicle. *Energies* **2022**, *15*, 1996.
44. Yao, J.; Wang, M.; Li, Z.; Jia, Y. Research on model predictive control for automobile active tilt based on active suspension. *Energies* **2021**, *14*, 671.
45. Youn, I.; Wu, L.; Youn, E.; Tomizuka, M. Attitude motion control of the active suspension system with tracking controller. *International Journal of Automotive Technology* **2015**, *16*, 593–601.